Benchmarking the HRP-2 humanoid robot during locomotion

Olivier Stasse, Kevin Giraud-Esclasse, Edouard Brousse, Maximilien Naveau, Rémi Régnier, Guillaume Avrin, Philippe Souères

frontiers

Benchmarking the HRP-2 humanoid robot during locomotion

Olivier Stasse [1,*], **Kevin Giraud-Esclasse** [1], **Edouard Brousse** [2], **Maximilien Naveau** [3], **Rémi Régnier** [2], **Guillaume Avrin** [2], **and Philippe Souères** [1]

[1] *Laboratoire d'Analyse et d'Architecture des Systèmes, (LAAS) CNRS, Université de Toulouse, France*
[2] *Laboratoire Nationale de Métrologie et d'essais (LNE), Paris, France*
[3] *Max-Planck Institute (MPI), Tuebingen, Germany*

Correspondence*:
Corresponding Author
ostasse@laas.fr

ABSTRACT

In this paper we report results from a campaign of measurement in a laboratory allowing to put a humanoid robot HRP-2 in a controlled environment. We have investigated the effect of temperature variations on the robot capabilities to walk. In order to benchmark various motions modalities and algorithms we computed a set of performance indicators for bipedal locomotion. The scope of the algorithms for motion generation evaluated here is rather large as it spans analytical solutions to numerical optimization approaches able to realize real-time walking or multi-contacts.

Keywords: benchmarking, bipedal locomotion, humanoid robot HRP-2, controlled environment, numerical optimization, walking

1 INTRODUCTION

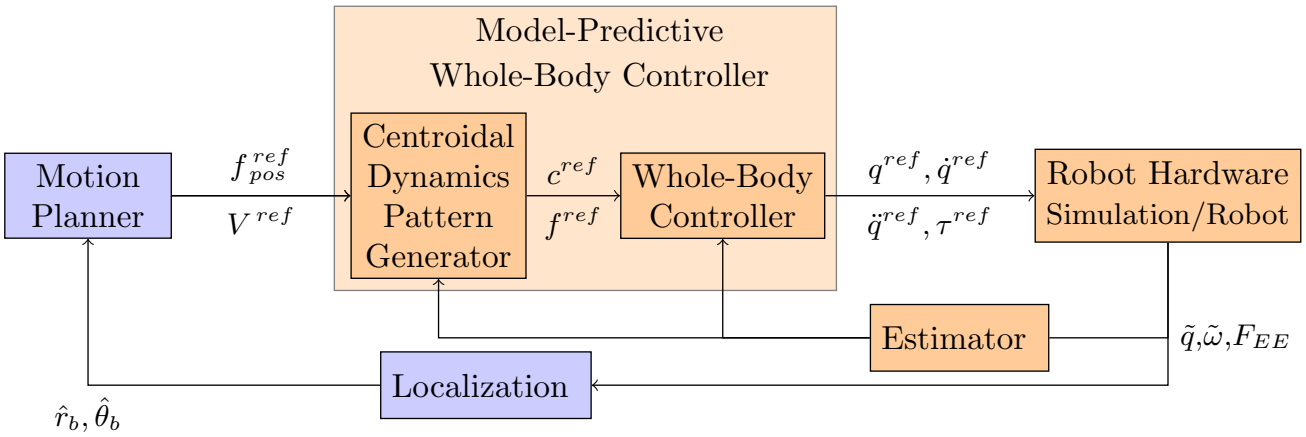

Figure 1. General architecture to generate motion for a humanoid robot. In this paper the boxes in orange are the one benchmarked, whereas the blue boxes are not benchmarked

From the seminal work of Chestnutt (2010) to the recent methods proposed in the frame of the Darpa Robotics Challenge (DRC) Tsagarakis et al. (2017); Lim et al. (2017); Radford et al. (2015); Johnson et al. (2017); Marion et al. (2017); DeDonato et al. (2017), humanoid robots are moving using a control architecture following the general framework depicted in Fig. 1. Based on an internal representation of the environment and the localization of the robot ($\hat{r}_b$ and $\hat{\theta}_b$ being respectively the base position and orientation), the **Motion Planner** (**MP**) plans a sequence of reference end-effector contact positions (f^{ref}), or a reference center of mass linear velocity combined with a reference waist angular velocity (V^{ref}). These references are then provided to a **Model-Predictive Whole-Body Controller** (**MPWBC**) which generates a motor command for each joint (joint torques (τ^{ref}), positions (q^{ref}), velocities ($\dot{q}^{ref}$) and accelerations ($\ddot{q}^{ref}$)). This block is critical in terms of safety as it maintains the dynamics feasibility of the control and the balance of the robot. The **Model-Predictive Whole-Body Controller** (**WBC**) can be expressed as a unique optimal control problem but at the cost of efficiency in terms of computation time or solution quality. This is why this controller is usually divided in two. First trajectories for the robot center of mass c^{ref} and the positions of contacts with the environment f^{ref} are found using a **Centroidal Dynamics Pattern Generator** (**CDPG**). And, in turn a **WBC** computes an instantaneous controller that tracks these trajectories. More details about the **CDPG** can be found in the next paragraph. The whole body reference is in turn sent to the **Robot Hardware**, which can be either the simulation or the real robot. The feedback terms are based upon the measurements of the different sensors. The encoders evaluate the joint position ($\tilde{q}$). The inertial measurement unit (IMU) measures the angular velocity ($\tilde{\omega}_{IMU}$) and the linear acceleration ($\tilde{a}_{IMU}$) of the robot torso, which give us information about the orientation of the robot with respect to the gravity field. Finally the interaction with the environment is provided by the force sensors classically located at the end-effectors ($F_{EE} \in \{F_{RF}, F_{LF}, F_{RH}, F_{LH}\}$ where the subscripts have the following meaning EE: end-effector, RF: right foot, LF: left foot, RH: right hand, LH: left hand). All these information are treated in an **Estimator** to extract the needed values for the different algorithm. Finally the **Localization** block is dedicated to locate as precisely as possible the robot in its 3D environment, Various implementations of this architecture have been proposed with various levels of success from the highly impressive Boston Dynamics System, to robots widely available such as Nao.

An open question is the robustness and the repeatability of such control system as well as its performance. In this paper we propose a benchmarking of the HRP-2 robot in various set-ups and provide performance indicators in scenarios which are possibly interesting for industrial scenarios.

The paper is structured as follows, first the paragraph 2 presents the related work on control and benchmarking for humanoid robots, then paragraph 3 depicts our precedent contribution in the Koroibot project and how it relates to this work, to continue, paragraph 4 lists the materials and different methods used to perform the benchmarking, in turn the paragraph 5 shows the experimental results using the indicators from paragraph 4, and finally the conclusion 6 summaries the contributions and results from this paper.

2 RELATED WORK

In this paragraph we present the work that has been done relative to the control and the benchmarking of humanoid robots.

2.0.1 Motion generation for humanoid robots

The different benchmarks included in this paper relate to **MPWBC** sketched in Fig. 1, so this section is dedicated to its related work. Several techniques are used to mathematically formulate this problem.

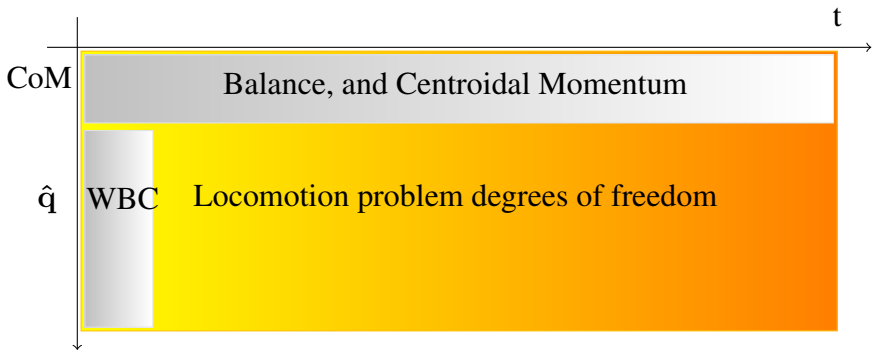

Figure 2. Representation of the size of the locomotion problem. The abscissa represent the duration of the predicted horizon and the ordinate the number of robot DoF.

For instance hybrid-dynamics formulations as proposed by Grizzle et al. (2010) or Westervelt et al. (2007) are efficient but difficult to generalize. The approaches used in this paper are based on mathematical optimization which is broadly used in the humanoid robotics community. More precisely, the problem of the locomotion can be described as an **Optimal Control Problem** (OCP). The robot generalized configuration (q^{ref}) and velocity ($\dot{q}^{ref}$) usually compose the state ($\mathbf{x}$). The future contact points can be precomputed by a **Motion Planner** or included in the state of the problem. The control of this system $\mathbf{u}$, can be the robot generalized acceleration ($\ddot{q}^{ref}$), the contact wrench (ϕ_k with $k \in \{0, \ldots, \text{Number of Contact}\}$), or the motor torques (τ^{ref}). We denote by $\underline{\mathbf{x}}$ and $\underline{\mathbf{u}}$ the state and control trajectories. The following optimal control problem (OCP) represents a generic form of the locomotion problem:

$$\min_{\underline{\mathbf{x}},\,\underline{\mathbf{u}}} \sum_{s=1}^{S} \int_{t_s}^{t_s+\Delta t_s} \ell_s(\mathbf{x},\mathbf{u})\,\mathbf{dt} \tag{1a}$$

$$s.t. \quad \forall t \quad \dot{\mathbf{x}} = dyn(\mathbf{x},\mathbf{u}) \tag{1b}$$

$$\forall t \quad \phi \in \mathcal{K} \tag{1c}$$

$$\forall t \quad \mathbf{x} \in \mathcal{B}_x \tag{1d}$$

$$\forall t \quad \mathbf{u} \in \mathcal{B}_u \tag{1e}$$

$$\mathbf{x}(0) = \mathbf{x}_0 \tag{1f}$$

$$\mathbf{x}(T) \in \mathcal{X}_* \tag{1g}$$

where $t_{s+1} = t_s + \Delta t_s$ is the starting time of the phase s (with $t_0 = 0$ and $t_S = T$). Constraint (1b) makes sure that the motion is dynamically consistent. Constraint (1c) enforces balance with respect to the contact model. Constraints (1d) and (1e) impose bounds on the state and the control. Constraint (1f) imposes the trajectory to start from a given state (estimated by the sensor of the real robot). Constraint (1g) imposes the terminal state to be viable Wieber (2008). The cost (1a) is decoupled $\ell_s(\mathbf{x},\mathbf{u}) = \ell_x(\mathbf{x}) + \ell_u(\mathbf{u})$ and its parameters may vary depending on the phase. ℓ_x is generally used to regularize and to smooth the state trajectory while ℓ_u tends to minimize the forces. The resulting control is stable as soon as ℓ_x comprehends the L_2 norm of the first order derivative of the robot center of mass (CoM), Wieber et al. (2015).

Problem (1) is difficult to solve in its generic form. And specifically (1b) is a challenging constraint. Most of the time the shape of the problem varies from one solver to another only by the formulation of this constraint. The difficulty is due to two main factors: 1) There is a large number of degrees of freedom

(DoF). In practice we need to compute 36 DoF for the robot on a preview window with 320 iterations ($1.6s$) to take into account the system inertia. 2) The system dynamics is non linear. Fig. 2 depicts the structure of problem. To be able to solve the whole problem, represented by the full rectangle in Fig. 2 researchers used nonlinear optimization. In this paper we evaluated a resolution of the **MPWBC** based on the formulation given by Eq. 1. In this approach described in Koch et al. (2014), the authors computed a dynamical step over motion with the HRP-2 robot, but this process can take several hours of computation. So simplifications are necessary, for example Tassa et al. (2014), Koenemann et al. (2015) uses simplifications on the contact model. This method is very efficient but is not suitable for complex contacts during walking for example. Seminal works (Orin et al. (2013),Kajita et al. (2003b)) show that (1b) can be divided in two parts, the non-convex centroidal dynamics (horizontal gray rectangle in Fig. 2) (Orin et al. (2013)) with few DoF and the convex joint dynamics (vertical gray rectangle in Fig. 2). Kuindersma et al. (2014) and Sherikov (2016) chose to deal the two gray part of Fig. 2 at once. They optimize for the centroidal momentum on a preview horizon and the next whole body control. Qiu et al. (2011), Rotella et al. (2015), Perrin et al. (2015) decouple the two separated gray rectangles in Fig. 2. They solve first for the centroidal momentum and then for the whole body control. In general the centroidal momentum is still difficult to handle due to its non-convexity. Finally Kajita et al. (2003a), Herdt et al. (2010), Sherikov et al. (2014) linearize the centroidal momentum which provides a convex formulation of the locomotion problem. In Deits and Tedrake (2014), the problem was formulated has a mixed-integer program (i.e. having both continuous and discrete variables) in case of flat contact. In Mordatch et al. (2012), the same problem was handled using a dedicated solver relying on a continuation heuristic, and used to animate the motion of virtual avatars.

2.1 Benchmarking

Different methods exist to benchmark robot control architectures, in del Pobil et al. (2006) the authors argue that robotic challenges are an efficient way to do so. For example, the results of the DARPA Robotics Challenge published in the Journal of Field Robotics special issues Iagnemma and Overholt (2015) and Spenko et al. (2017), show the different control architecture in a determined context. Each behavior successfully accomplished grants point to the team and the best team won the challenge. This benchmarking was however costly as the robots had no system to support them in case of fall. In addition, as it is mostly application driven it is necessary in evaluating the system integration but not the independent subparts.

For the specific case of motion generation, it has been recently proposed by Brandao et al. (2017) to use a scenario called "Disaster Scenario Dataset". It allows benchmarking posture generation (solved by the **WBC**) and trajectory generation (**MPWBC**) using optimization. A set of problems is proposed by means of foot steps locations(F_{RF}, F_{LF}). From this it is possible to compare algorithms realizing the two functionnalities (**WBC** and **MPWBC**). The evaluation is realized in simulation using the Atlas robot and the ODE dynamic simulator. This first step is necessary but one step further is to benchmark a real humanoid platform. For this paper we used a more systematic decomposition of the humanoid bipedal locomotion Torricelli et al. (2015). Further description can be found in paragraph 4.7. This paper focuses on evaluating the **MPWBC** and **WBC** on the **Robot Hardware**. The **Estimator** used in this context is important but it is reflected in the stabilization process. The **Motion Planning** is not evaluated here as the planned motion is always the same or solved at the **MPWBC** level. The **Localization** is provided by a motion capture system.

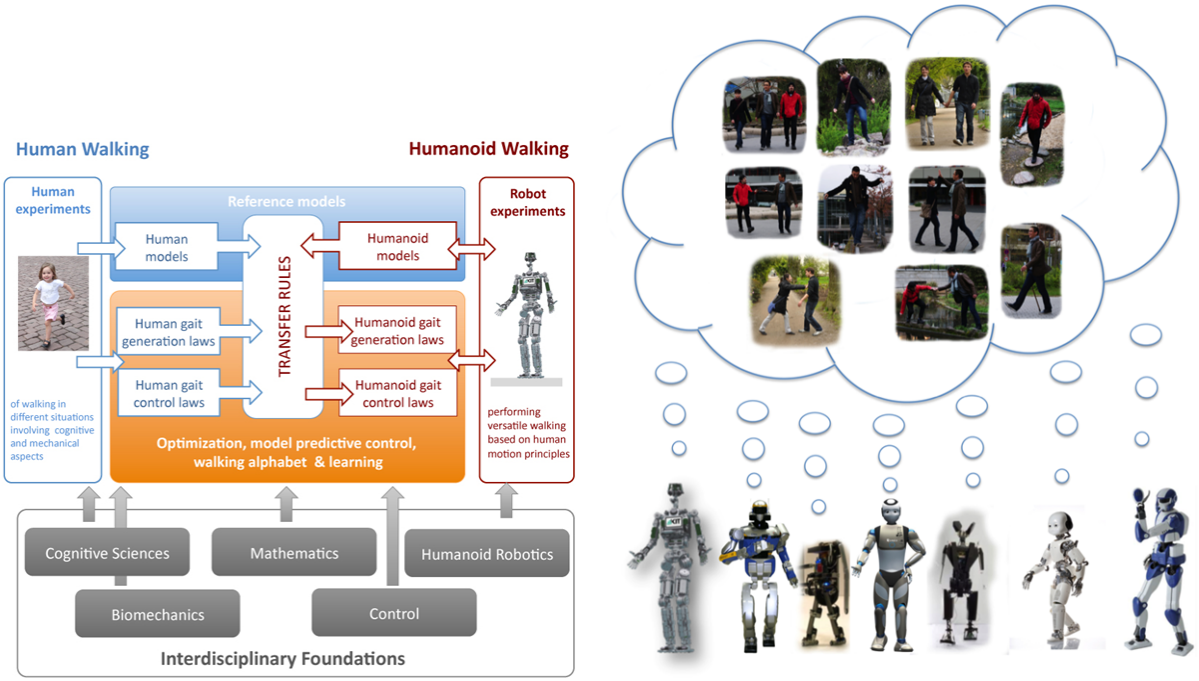

Figure 3. (left) Graphical representation of the scientific approach of the Koroibot project - (right) View of the humanoid robot used in the Koroibot project dreaming of human walking capabilities

3 THE KOROIBOT PROJECT AND OUR PRIOR CONTRIBUTIONS

The work presented in this paper takes its root in the context of the European project Koroibot (`http://www.koroibot.eu/`).

3.0.1 General purpose

The goal of the Koroibot project was to enhance the ability of humanoid robots to walk in a dynamic and versatile way, and to bring them closer to human capabilities. As depicted in Fig. 3-(left), the Koroibot project partners had to study human motions and use this knowledge to control humanoid robots via optimal control methods. Human motions were recorded with motion capture systems and stored in an open source data base which can be found at `https://koroibot-motion-database.humanoids.kit.edu/`. With these data several possibilities were exploited:

- Criteria that humans are assumed to minimize using Inverse optimal control.
- Transfer from human behaviors to robots was done with walking alphabets and learning methods Mandery et al. (2016).
- These human behavior was safely integrated in robots applying optimal controllers.
- Design principles were derived for new humanoid robots. Mukovskiy et al. (2017); Clever et al. (2017)

3.0.2 The robot challenges

In order to evaluate the progress of the algorithms at the beginning and at the end of the project, a set of challenges were designed focusing specifically on walking (see Fig. 4). Fig. 3-(right) shows all the robot hosted by the various partners. All the team owning a robot had to perform some of these challenges considering the current and potential state of their robots and controllers.

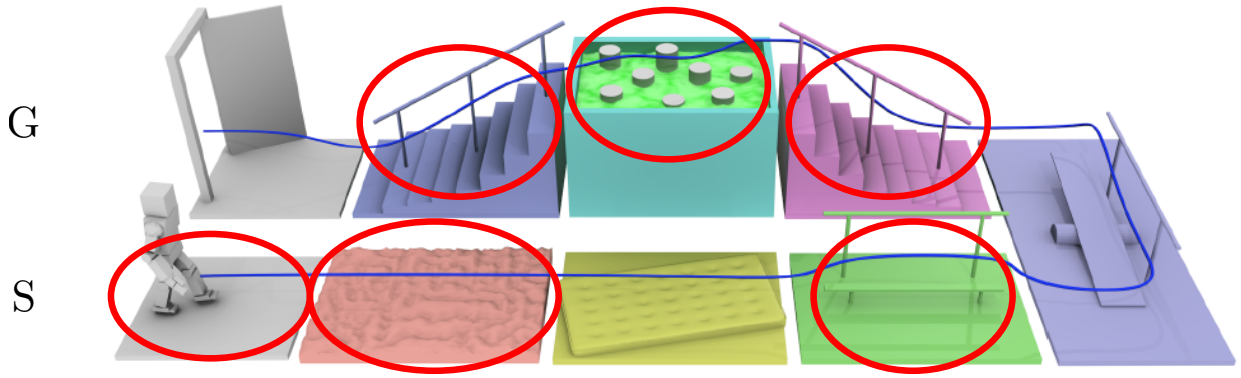

Figure 4. Challenges of the Koroibot project. In red the challenges chosen by the LAAS-CNRS.

3.0.3 The Key Performance Indicators (KPI)

In this context and in collaboration with the H2R project, a detailed set of key performance indicators (KPI) have been proposed Torricelli et al. (2015). These KPI try to capture all the bipedal locomotion patterns. Specific sub-functions of the global motor behaviors were analyzed (see Fig. 5-(right)). The results are expressed as two different sub-function sets. First, the sub-functions associated to body posture task with no locomotion. And second the same sub-functions but including the robot body transport. The initial condition may vary depending on the experiment to perform. This is the idea of the intertrial variability. The sub-functions are also classified by taking into account the changes in the environment or not. Each of these functions can be evaluated for different robots using the criteria depicted in Fig. 5-(left). The performance are classified in two sub categories, quantitative performance and human likeness. In addition there are indications on the last two columns if the criteria is applicable on a standing task or on a locomotion task. Again, all the team owning a robot had had to perform an evaluation of these KPI, considering the current and potential state of their robots and controllers.

3.1 The work done in the Koroibot context

In the Koroibot context the gepetto team evaluated the KPI one the robot HRP-2 (second robot from the left in (Fig. 3-(right)). Among the challenges presented in Fig. 4, we considered the following ones:

- walking on a flat ground,
- walking on an uneven ground,
- walking on a mattress,
- walking on a beam without handrail,
- climbing a stair case with/without handrail,
- walking on stepping stones,
- going down a stair case without handrail,

They are depicted by red circles in Fig. 4. In addition to these challenges we added the perturbation rejection. Considering the selected challenges we picked the following KPI sub-function:

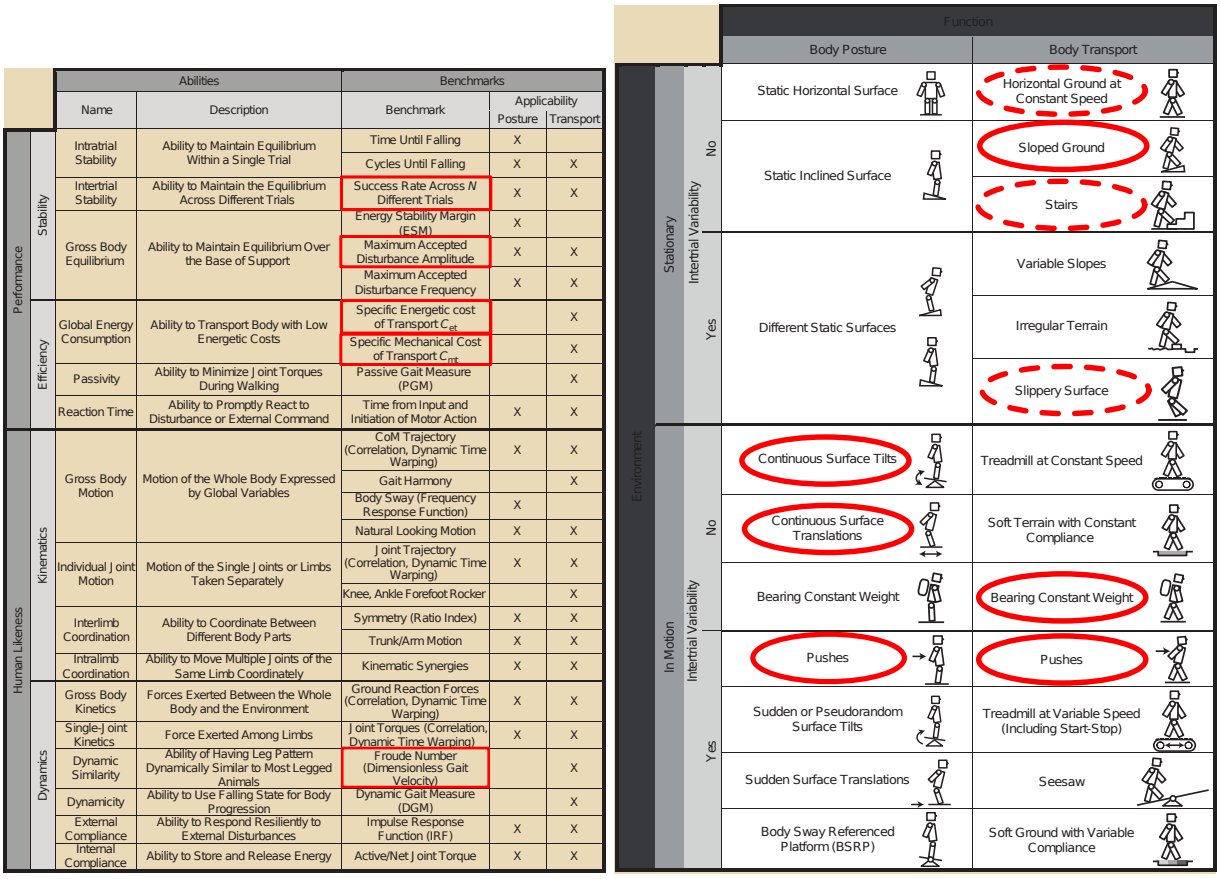

		Abilities		Benchmarks		
		Name	Description	Benchmark	Applicability Posture	Applicability Transport
Performance	Stability	Intratrial Stability	Ability to Maintain Equilibrium Within a Single Trial	Time Until Falling	X	
				Cycles Until Falling	X	X
		Intertrial Stability	Ability to Maintain the Equilibrium Across Different Trials	Success Rate Across *N* Different Trials	X	X
		Gross Body Equilibrium	Ability to Maintain Equilibrium Over the Base of Support	Energy Stability Margin (ESM)	X	
				Maximum Accepted Disturbance Amplitude	X	X
				Maximum Accepted Disturbance Frequency	X	X
	Efficiency	Global Energy Consumption	Ability to Transport Body with Low Energetic Costs	Specific Energetic cost of Transport C_{et}		X
				Specific Mechanical Cost of Transport C_{mt}		X
		Passivity	Ability to Minimize Joint Torques During Walking	Passive Gait Measure (PGM)		X
		Reaction Time	Ability to Promptly React to Disturbance or External Command	Time from Input and Initiation of Motor Action	X	X
Human Likeness	Kinematics	Gross Body Motion	Motion of the Whole Body Expressed by Global Variables	CoM Trajectory (Correlation, Dynamic Time Warping)	X	X
				Gait Harmony		X
				Body Sway (Frequency Response Function)	X	
				Natural Looking Motion	X	X
		Individual Joint Motion	Motion of the Single Joints or Limbs Taken Separately	Joint Trajectory (Correlation, Dynamic Time Warping)	X	X
				Knee, Ankle Forefoot Rocker		X
		Interlimb Coordination	Ability to Coordinate Between Different Body Parts	Symmetry (Ratio Index)	X	X
				Trunk/Arm Motion	X	X
		Intralimb Coordination	Ability to Move Multiple Joints of the Same Limb Coordinately	Kinematic Synergies	X	X
	Dynamics	Gross Body Kinetics	Forces Exerted Between the Whole Body and the Environment	Ground Reaction Forces (Correlation, Dynamic Time Warping)	X	X
		Single-Joint Kinetics	Force Exerted Among Limbs	Joint Torques (Correlation, Dynamic Time Warping)	X	X
		Dynamic Similarity	Ability of Having Leg Pattern Dynamically Similar to Most Legged Animals	Froude Number (Dimensionless Gait Velocity)		X
		Dynamicity	Ability to Use Falling State for Body Progression	Dynamic Gait Measure (DGM)		X
		External Compliance	Ability to Respond Resiliently to External Disturbances	Impulse Response Function (IRF)	X	X
		Internal Compliance	Ability to Store and Release Energy	Active/Net Joint Torque	X	X

Figure 5. (left) Performances indicators (right) The motor skills considered in the benchmarking scheme. This scheme is limited to bipedal locomotion skills. The concept of intertrial variability represent modifications of the environment between trials. (dashed) Motor skills evaluated in Naveau (2016) (not dashed) Motor skills evaluates in this paper.

- horizontal ground at constant speed,
- stairs,
- bearing constant weight (the robot's own weight)
- success rate across N different trials,
- mechanical energy,
- mechanical plus electrical energy,

All these choices are shown in Fig. 5 by red ellipses on the table. The mathematical details and results are presented below in paragraph 4.7.

4 MATERIALS AND METHODS

In this paragraph the experimental setups used to compute each of the performance indicators given in 4.7 are described. It also presents the motor skills given in Fig. 5 and their implementation. In addition to this, the algorithms used to perform the different test are depicted in paragraph 4.8.

4.1 Different temperatures

LNE is equipped with temperature varying rooms which allowed us to quantify some of the performance indicators between $5°C$ and $45°C$. In this way, we evaluated the robustness and limits of our robot for all

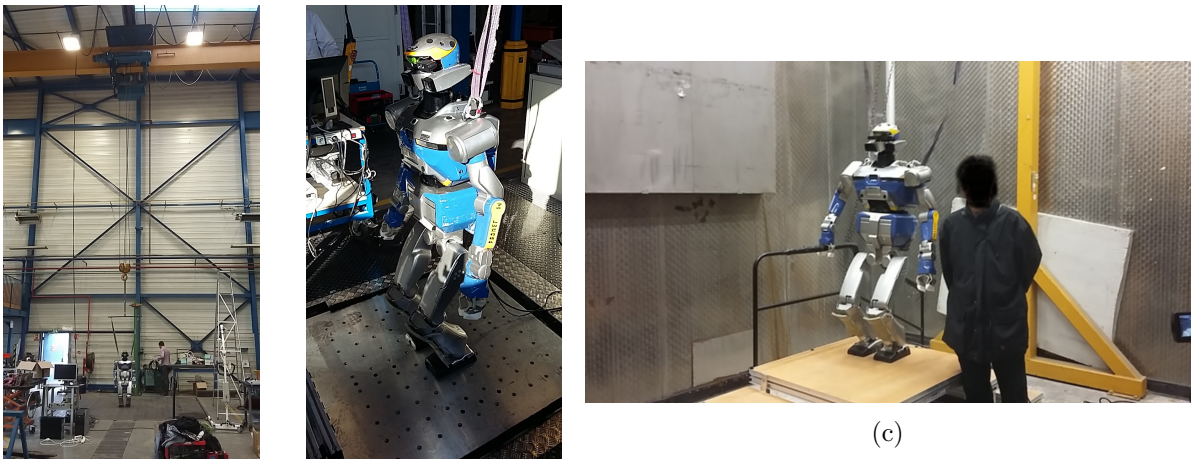

(a) (b) (c)

Figure 6. Pictures of the experimental setup at LNE (a) the robot hang up to walk on a slope (b) the translational plate (c) the temperature controlled chamber (end of the robot climbing $15\ cm$ at $10°C$)

the performance indicators. It appeared that the robot behavior deteriorates at low temperatures. At $5°C$ it was not possible to perform the calibration procedure as the robot could not move. At $10°C$ the friction are sufficiently low such that the robot could move. Another phenomena occurs above $40°C$: thermal protection prevents the robot from moving if the temperature is too high. This happens at $40°C$ after few motions due to internal temperature build up. In this room, apart from these extreme cases, the motions and indicators measurements have be performed as expected on a flat ground or on the stairs from the Koroibot project. This staircase is made of 4 stairs and a platform with each stair separated by $15\ cm$ height. The dimension of one stair case is $1\ m \times 0.25\ m \times 0.05\ cm$.

4.2 Tilted surfaces

In the context of the body skills in motion, we considered tilting surfaces. This was tested with the stabilizer commercially available with HRP-2. The setup is a platform which can be tilted upward and downward on one side with an hydraulic actuator. The surface was tilted continuously until the robot fell off. On the other hand, we tested walking algorithms with different angles (pointing up or down) until the robot fell down. Tests were realized with the robot pointing down, pointing up and across the slope. In Fig. 5 this corresponds to Body Posture - Continuous Surface Tilts.

4.3 Horizontal translations

We used a mobile plate controlled in the horizontal plane to perform continuous oscillating surface translations at various frequencies and various amplitudes. The platform was using a hydraulic actuator. The aim was to find the frequency and the amplitude that the controlled robot is able to sustain. In Fig. 5 this corresponds to Body Posture - Continuous Surface translations.

4.4 Bearing

In order to test bearing weights with the robot, we added bags of $5\ kgs$ to $15\ kgs$ in such way that the robot balance is maintained. This approach is a bit limited as they are several ways to bear a weight. Indeed it can be done with a backpack, in collaboration with someone, by holding the object against its chest. Each

of this approach comes with its own specific constraint. In order to avoid such constraints, we decided to take the most simplest choice and hang soft weights on the front and the back of the chest. In Fig. 5 this corresponds to Body Transport - Bearing Constant Weight.

4.5 Pushes

This paragraph presents the pushes experiments. We tried to find the sufficient force to make the robot fall down. This was achieved by using a stick on top of which was fixed a force sensor displaying the maximum force measured during a physical interaction. The experience was realized while the robot was standing and walking. The force was applied in the sagittal and frontal planes until making HRP-2 fall. The force was applied behind the waist of the robot. This part of HRP-2 was made specifically soft to support impacts. The walking part is the most difficult in terms of repeatability as the robot might be in different foot support and therefore be less stable depending on the situation. In Fig. 5 this corresponds to Body Posture - Pushes and Body Transport - Pushes.

4.6 Data

A CAD model of this staircase used is available on the github repository where all the log of the experiments are also present: https://github.com/laas/koroibot_KPI. All the computation performed on the logs and implementing the key performance indicators are available here: https://github.com/laas/EnergyComputation.

4.7 Key Performance indicators (KPI)

In this section the performance indicators used to evaluate the humanoid robot HRP-2 are described. They are mostly based on the work proposed in Torricelli et al. (2015). In the Koroibot project we used key

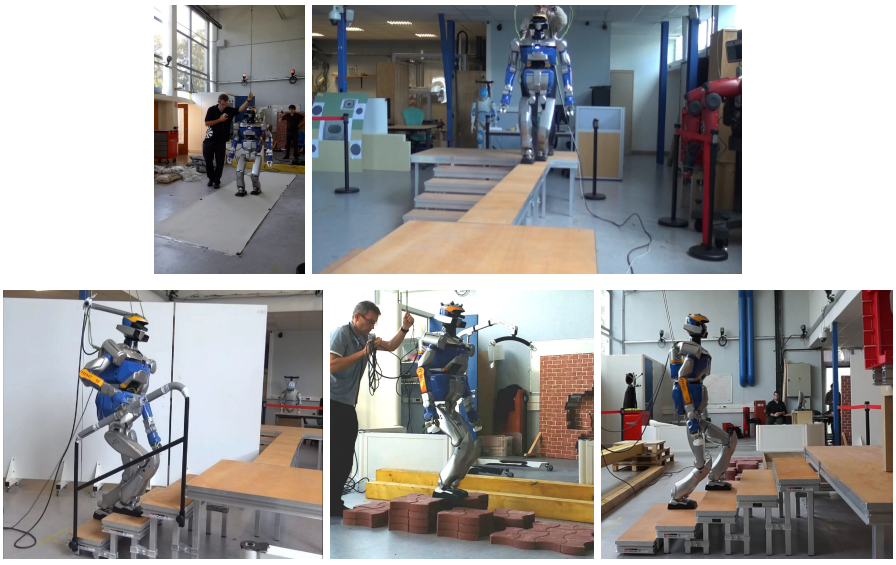

Figure 7. Sample of the experimental setup of the Koroibot project in LAAS-CNRS

performance indicators (KPI) to analyze the behavior of the robot at the beginning and at the end of the project. These results lead us toward the improvements to be made. In 2013 the algorithm mostly used and implemented on HRP-2 in LAAS-CNRS where the walking pattern generators described in Morisawa et al. (2007) and in Herdt et al. (2010). The performance indicators chosen were:

- The execution time $T_M = t_{end} - t_{begin}$, where t_{begin} is found when the sum of the norm of the motor axis velocities reaches $6\,rad\ s^{-1}$ for the first time in the log and t_{end} is when the sum of the norm of the motor axis velocities is below $0.5\,rad\ s^{-1}$.
- The walked distance, being the distance between the final base position and the first one. The base pose is reconstructed using an odometry with the joint positions only. The drift of this odometry is $8cm$ over a $3.6m$ during a straight walk.
- The success rate, being the number of time a specific task could be performed without fall, over the total number of trial of the task.
- The maximum tracking error from the planned trajectory,

$$TrackingError(t) = \int_{t}^{t+0.1} |q^{ref} - \tilde{q}|dt/0.1$$
$$MaxTrackingError = \max_{t}(TrackingError(t))$$

  with $TrackingError$ being the average normed difference between the desired joint trajectory (q^{ref}) and the joint pose measured from the encoder ($\tilde{q}$) during $0.1s$ starting at time t. And $MaxTrackingError$ being the maximum value of the $TrackingError$ function.
- The mechanical energy consumed normalized over the walking distance D and the execution time T_M.

$$E_{mechanical} = \int_{t_{begin}}^{t_{end}} |\tau\omega|dt/(T_M\ D)$$

  with $E_{mechanical}$ being the integral over time of the mechanical power, τ being the torques applied at the robot joints and ω being the velocity of the robot joints
- The electrical energy dissipated by the motor resistance normalized over the walking distance D and the execution time T_M,

$$E_{motor\,resistance} = \int_{t_{begin}}^{t_{end}} R\ i^2 dt/(T_M\ D) = \int_{t_{begin}}^{t_{end}} R\ k_c^2\ \tau^2 dt/(T_M\ D)$$

  with $E_{motor\,resistance}$ being the integral over time of the electric power dissipated, R being the motor resistances, k_c being the electric motor torque constant and τ being again the torques applied at the robot joints.
- The total energy consumed during the walking distance D and the execution time T_M,

$$E_{total} = E_{mechanical} + E_{motor\,resistance} + E_{electronics}$$

  with E_{total} being the sum of the energy consumed by the system normalized over the walking distance D and the execution time T_M, and $E_{electronics}$ being the energy consumed by the on-board electronic cards. $E_{electronics}$ is neglected in this study so:

$$E_{total} = E_{mechanical} + E_{motor\,resistance}$$

- The mechanical cost of transport and the total cost of transport,

$$E_{mechanical\,cost\,transport} = \int_{t_{begin}}^{t_{end}} |\tau\omega| dt/(m\ g\ D)$$

$$E_{total\,cost\,transport} = \left(\int_{t_{begin}}^{t_{end}} |\tau\omega| dt + \int_{t_{begin}}^{t_{end}} R\ k_c^2\ \tau^2 dt \right) /(m\ g\ D)$$

with $E_{mechanical\,cost\,transport}$ and $E_{total\,cost\,transport}$ being the respectively the mechanical and total cost of transport, m being the total mass of the robot, and $g = 9.81 ms^{-2}$ the gravity constant.

- The Froude number,

$$F_r = \frac{v}{\sqrt{gl}}$$

$$v = \frac{D}{T_M}$$

where v is the robot center of mass mean velocity along the horizontal plane,, and l is the leg length. This number represents the ratio between the kinetic energy and the potential energy. It can also be interpreted as an indicator on the stepping frequency.

The trajectories were generated off line and repeatedly played on the robot to analyze their robustness. Views of the experimental setups can be seen in Fig. 7.

4.8 Motion generation for humanoid robots locomotion

This section explains the links between the motion generation architecture depicted in Fig.1 and the Key Performance Indicators given in the paragraph 4.7. The set of function entitled body posture depicted in Fig.1-(right) represents the behavior which is provided by what is called a whole-body controller. It consists in two parts:

- an estimator, which provides the orientation of the robot with respect to the gravity field and the positions of the end-effectors in contact with the environment.
- a whole-body controller which guarantee that the robot balance is maintained with respect to c^{ref}, f^{ref} and possibly a q^{ref}.

In this paper we have evaluated independently only one whole body motion controller. It is the stabilizer provided by Kawada Inc. We give detailed performances evaluation of this controller in the experimental part of this paper. It was described in various paper such as Kajita et al. (2007) and Kajita et al. (2001).

The set of function entitled body transport depicted in Fig.1-(right) in this paper are four **CDPG** and one **MPWBC**. The four **CDPG** evaluated in this paper are the following ones: Carpentier et al. (2016), a multi-contact centroidal dynamic pattern generator used to climb stairs with given contact positions, Kajita et al. (2003a) the original walking pattern generator implemented by Shuuji Kajita with given foot steps, Morisawa et al. (2007) an analytical walking pattern generator allowing immediate foot step modifications, Naveau et al. (2017) a real time non linear pattern generator able to decide autonomously foot-steps positions. In each case the goal of the **CDPG** is to generate a center of mass trajectory and the foot-steps trajectories. For Kajita et al. (2003a), Naveau et al. (2017), and Morisawa et al. (2007) a dynamical filter is used to correct the center of mass trajectory to improve the dynamical consistency of

the motion. In each case, a whole body motion generator (not to be confused with a whole body motion controller) is used without feedback to generate the reference position q^{ref}, and the desired z^{ref} which is then send to the stabilizer. For Naveau et al. (2017) and Morisawa et al. (2007) we used the stack of task described in Mansard et al. (2009) as a Generalized Inverse Kinematics scheme. In Carpentier et al. (2016) a Generalized Inverse Dynamics was used to generate the reference value for q^{ref} and c^{ref}. The **MPWBC** provides directly the controls. The one used is from Koch et al. (2014) using the Muscod-II Diehl et al. (2001) nonlinear solver.

5 EXPERIMENTS

In this paragraph we present the numerical results obtained from the computation of the KPI explained in details in paragraph 4.7 for each set of experiments. As a reminder here the list of the KPI:

- walked distance,
- success rate,
- max tracking error,
- duration of the experiment,
- mechanical joint energy,
- actuators energy,
- cost of transport,
- mechanical cost of transport,
- Froude number.

A video displaying a mosaic of all the experiments is available at the following URL: https://www.youtube.com/watch?v=djWGsb44JmY&feature=youtu.be.

5.1 Climbing stairs

5.1.1 Stairs of 10 cm

In this experiment, the humanoid robot HRP-2 is climbing stairs of $10\ cm$ height without any handrail. The difficulty of this task is that the robot has to do quite large steps and to perform vertical motion. Because of the large motion issue the robot is climbing one stair at a time. Which means that the robot put one foot on the next stair and the other on the same stair. This avoid a too large joint velocity that the robot could not track.

Morisawa et al. (2007) **CDPG** was evaluated at the beginning of the project although the variation of height violates the assumption of the cart table model. But thanks to the dynamical filter the motion generated was sufficiently dynamically consistent so that the stabilizer could cope with the situation. The test was performed in a room at $20°C$. The KPI results can be seen in Fig. 11-(tool upstairs).

The other test was performed at the end of the project on the **CDPG** Carpentier et al. (2016). This time the **CDPG** took into account the center of mass height variation but not the whole body motion. The stabilizer should theoretically less trouble to compensate for the simplifications made. For Carpentier et al. (2016) three different temperatures were tested: $10°C$, $20°C$ and $35°C$. The numerical results are depicted in Fig. 8.

Interestingly, the temperature level has a direct impact in terms of mechanical cost as it diminishes with the increase in temperature. It is reflected in the tracking error. This intertrial variation do not come from

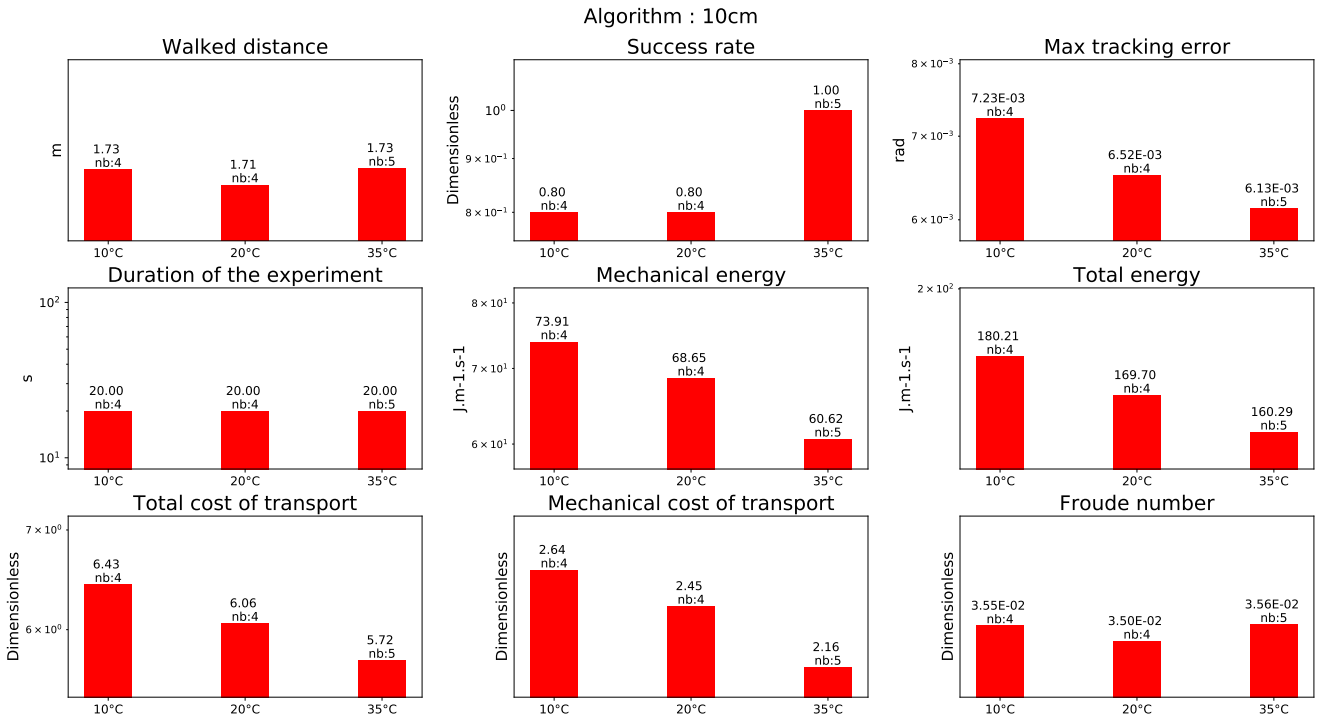

Figure 8. Climbing $10\ cm$ stairs without handrail

the change of reference trajectory as it is strictly the same for every trial. There is a level of adaptation due to the stabilizer, but each temperature has been tested at least 4 times. A possible explanation is the fact that the grease in the harmonic drive generate less friction with higher temperature.

As the cost of transport is dimensionless it allows to compare the two motions regardless of their duration. It is then interesting to see that the cost of transport in Fig. 11-(tool upstairs) and in Fig. 8-($10°C$) are very similar. And that at the same temperature the total cost of transport for Carpentier et al. (2016) **CDPG** is 9.6% better (from 6.71 to 6.06). One explanation is that the motion from Carpentier et al. (2016) **CDPG** being more dynamically consistent, the stabilizer consume less energy to compensate for the model simplifications.

5.1.2 Stairs of $15\ cm$

In this experiment, the humanoid robot HRP-2 is climbing stairs of $15\ cm$ height using a handrail. In addition the robot is not using any stabilization algorithm, because there are non-coplanar contacts.

In this setup the Morisawa et al. (2007) **CDPG** has to be used without handrail because of the model simplifications. Trials has therefore been done using a **WBC** (described in Mansard et al. (2009)) without the handrail. The results show that the current demanded by the motors went up to $45\ A$. And because the HRP-2 batteries can not provide more than $32\ A$, all trial failed. This is the reason why the results are not shown in this study.

Nevertheless, tests using the handrail could be performed with Carpentier et al. (2016) **CDPG**. The corresponding results are depicted in Fig. 9. It confirms that the energy is decreasing with the increase of temperature without the stabilizer. Note that the energy spend by the robot is clearly higher than for the experience on the $10\ cm$ stairs, i.e. a 36% of increase for the energy of walking.

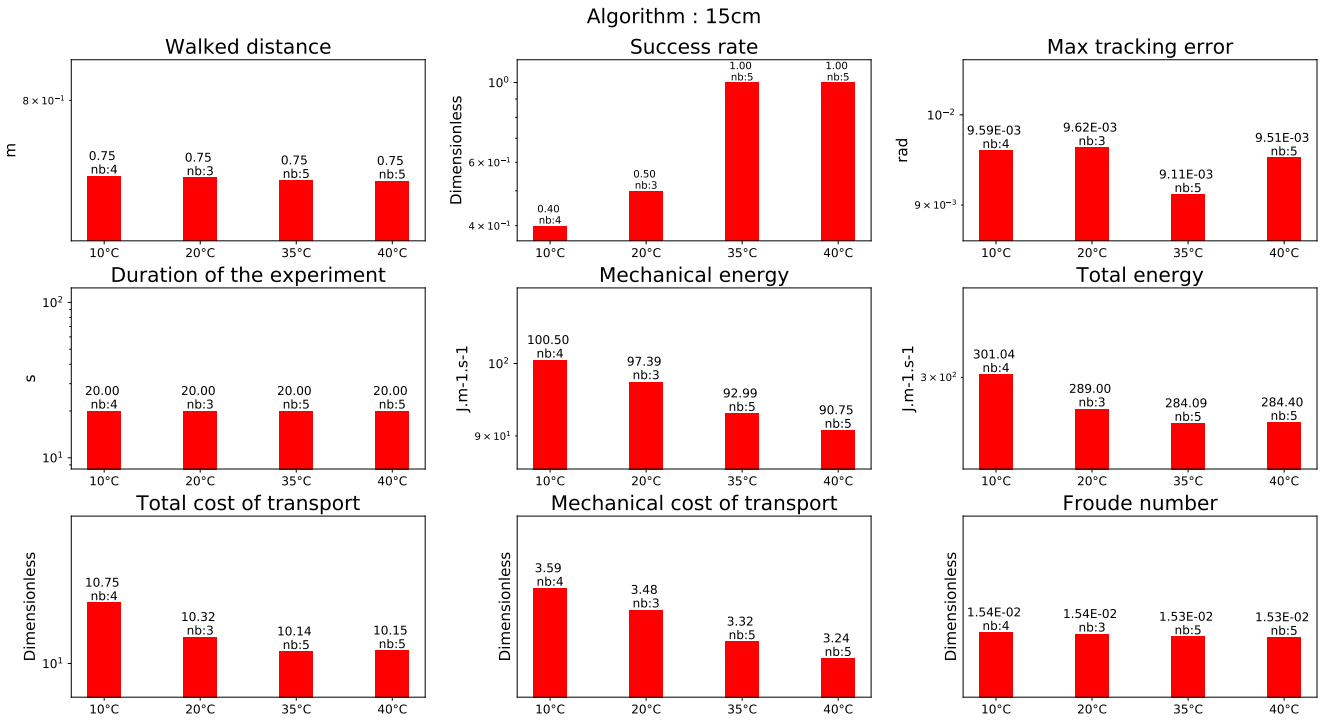

Figure 9. Climbing $15\ cm$ stairs with a handrail

5.1.3 Stepping Stones

In this experience, the humanoid robot HRP-2 had to go up and down on stairs made of red interlocking paving stones. Between each stairs there is a height difference of $\pm 5\ cm$. It is using the **CDPG** described in Morisawa et al. (2007). It is slightly different from the previous experiments because there are holes between the stairs. To cope with this, the generated trajectories had to always change the height of the next support foot. As the paving stones were always slightly moving due to the robot weight the balance was difficult to obtain in a reliable way. As indicated in the graph depicted in Fig.11, despite a success rate of 1, the tracking error reaches a level ($8e^{-03}$). This tracking error is greater than the one obtained by the $10\ cm$ climbing experiment at $10°C$ but lower than the one obtained by the $15\ cm$ climbing experiment at $35°C$ (which is the lower for this temperature and the **CDPG**). A possible explanation why the energy consumption is greater is greater than the $10\ cm$ climbing stairs is mostly due to the unstability of the stones and the fact that in this experiment the robot climb the stairs in a human fashion, i.e not one stair at a time.

5.2 Walking on a beam

This experiments was realized using the **CDPG** Morisawa et al. (2007). In this experiment the humanoid robot HRP-2 is walking on a beam. Initially, the experiment success rate on a real beam was around $20\,\%$. This rate was improved to achieve a $90\,\%$ success rate, thanks a new implementation of the dynamical filter presented in Kajita et al. (2003a). It reduced the drift which is important as the beam length is $3\,m$ long. This could be probably improved by a proper vision feed-back. In this study though the robot walked on a normal ground as if it where on a beam. The reason is the absence of a beam in the temperature controlled room. This means that the balance problem is exactly the same though the precision of the foot

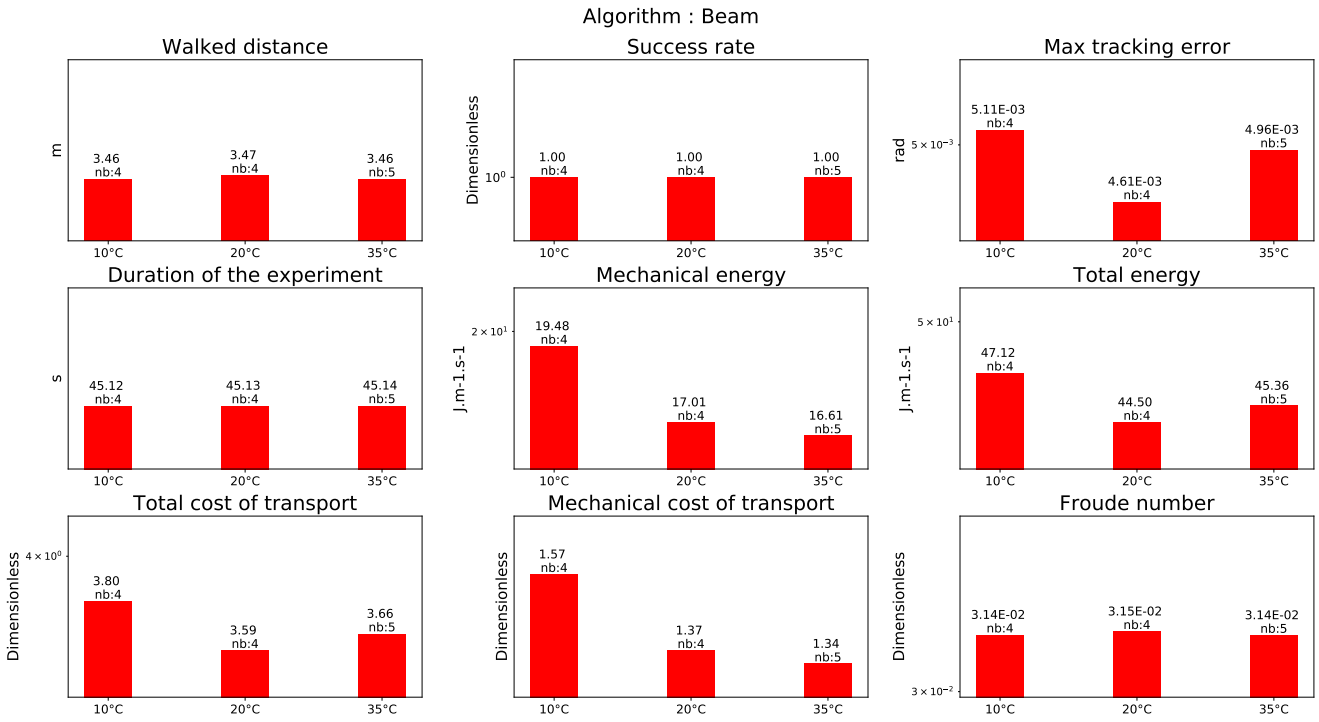

Figure 10. Walking on a beam

step location is discarded. Hence in this study the success rate is 1. The corresponding result is depicted in Fig. 10.

To perform the motion, the robot has to execute faster motions with its legs than compare to straight walking. It is emphasized by the increase of the cost of transport compared to normal straight walking (see Fig.13). Though the robot's leg are moving faster, the step frequency is lowered compared to a normal walking in order to keep the joint velocities in the feasible boundaries. This is reflected by the fact that the Froude number is around 35% less that a straight walking one (see Fig.13).

5.3 Straight flat ground walking

5.3.1 Temperatures

In the temperature controlled room the humanoid robot HRP-2 is performing a $2\,m$ straight walking following the implementation of Kajita et al. (2003a). The corresponding result is depicted in Fig. 13. Note that the energy with respect to the temperature is following the same trend as for the experiments on the stairs and on the beam.

We also tested the algorithm Naveau et al. (2017) at $10°C$. The total cost of transport is higher than the algorithm Kajita et al. (2003a) at the same temperature but lower than the one used for going over the beam. It is however largely less than the total cost of transport for climbing stairs at $10°C$.

The fact that the energy cost is higher for Naveau et al. (2017) than for Kajita et al. (2003a) at the same temperature is that Naveau et al. (2017) provide a higher range of motion but the generated motion are closer to the limit of the system, so the stabilizer spend more energy to compensate for this.

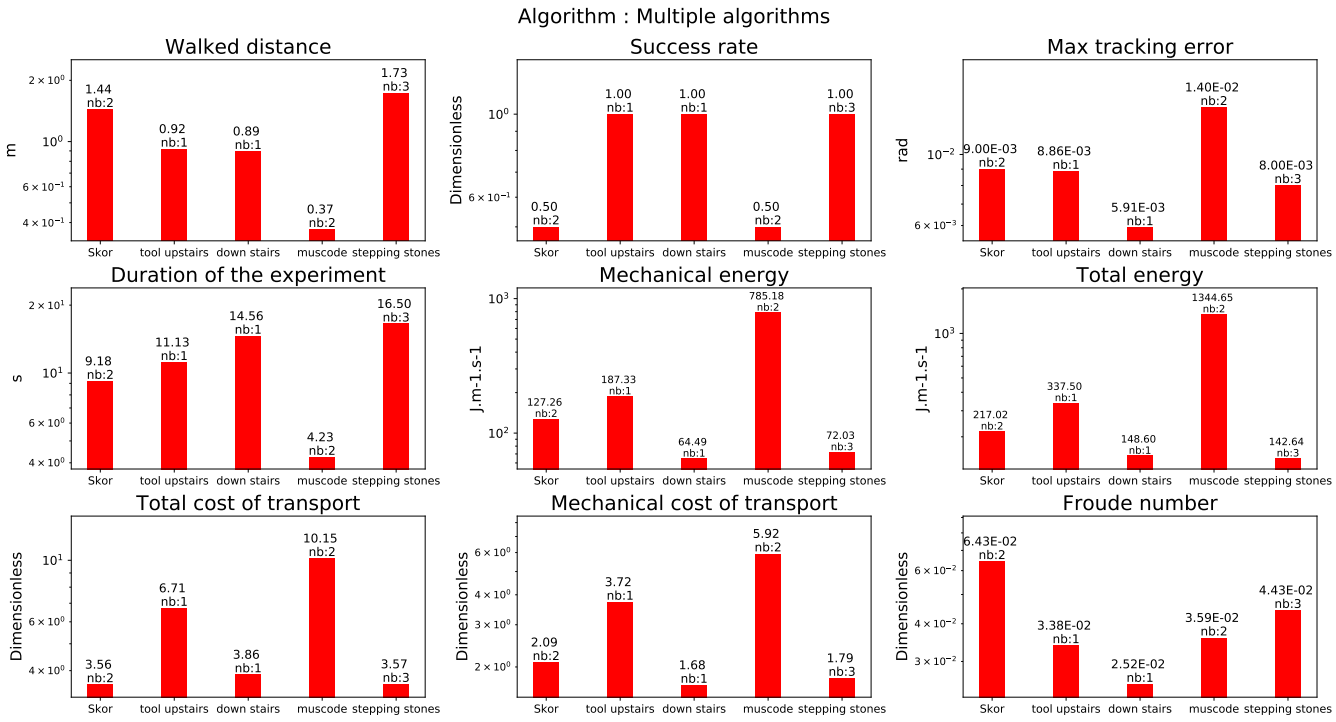

Figure 11. Multiple algorithms: going up with a tool on a wooden pallet $10\ cm$ (tool upstairs), going down on a wooden pallet $10\ cm$(down stairs), going over an obstacle solving an **OCP** approach (muscode), stepping on a interlocking paving stones (stepping stones)

5.3.2 Bearing weights

We made the humanoid robot HRP-2 walks while bearing weights at ambient temperature between $15°$ and $19°$. The two algorithms Kajita et al. (2003a) and Naveau et al. (2017) were tested. The robot was able to walk while carrying up to $14\ kg$ for the two algorithms. Note that, as expected, the effort to compensate for the additional weight reflects in the cost of transport.

5.3.3 Pushes

We performed pushes in the lateral direction and in the frontal direction while the robot was walking along a straight line. The two algorithms Kajita et al. (2003a) and Naveau et al. (2017) were again tested. In our case, the tested algorithm was not able to modify its foot-steps according to the pushes in contrary to the impressive work of Takumi et al. (2017). For this specific set of experiments with push from the back, the robot was able to sustain forces from $31\ N$ to $47\ N$. Pushes applied in the lateral plane were varying from $23\ N$ to $40\ N$. For Kajita et al. (2003a), the cost of transport has a value of 3.31 similar to the beam behavior. It is lower than the cost of transport for climbing stairs. The cost of transport for Naveau et al. (2017) is of 4.08. For both algorithms pushes are among the most consuming behaviors. It is due to the stabilizer compensating for the perturbation.

5.3.4 Slopes

The robot walked on a straight line while being on a slope of various angles ($[1° - 3.0°]$) -and with two possible directions (upward or downward). The two algorithms Kajita et al. (2003a) and Morisawa et al. (2007) were tested. For Kajita et al. (2003a) the cost of transport is higher than standard straight walking

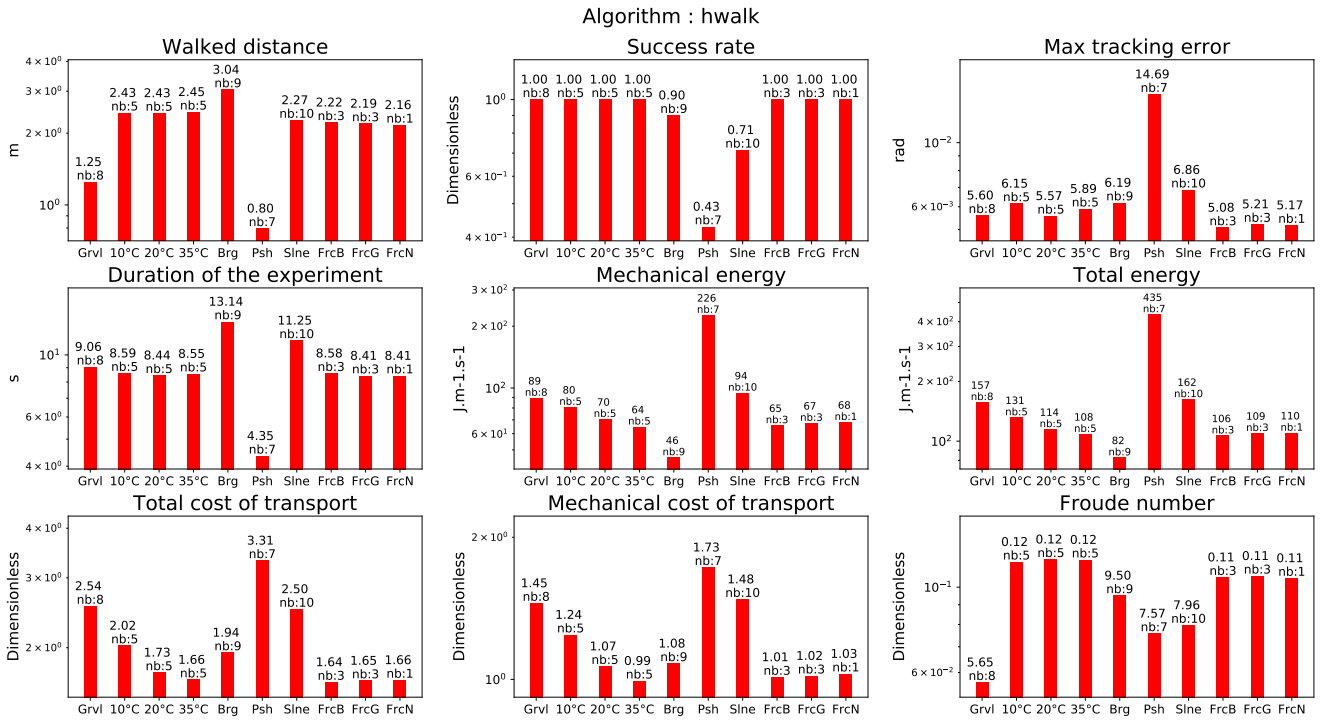

Figure 12. Straight walk with Kajita's walking pattern generator Kajita et al. (2003a)

but far less than during the pushes. For Morisawa et al. (2007) the cost of transport is higher than even the pushes for Kajita et al. (2003a) and the same level than the beam. It can be explained by the fact that when the experiment has been realized the dynamical filter was not used. Therefore the stabilizer had to compensate for the discrepancy between the motion dynamic and the reference of the center of pressure. An algorithm able to estimate the ground slope and adapt to it would probably increase the efficiency of this motion.

5.3.5 Frictions

The robot walked on carpets with different textures implying different friction coefficients bought in a home center. In this case, we did no see any consequences with the **CDPG** Kajita et al. (2003a). This is probably due to the particular shape of the soils which is one way to affect the friction coefficient. A possible extension of this work would be to use more slippery ground. But a proper way to handle such case is to implement a slip observer such as it was done Kaneko et al. (2005).

5.3.6 Uneven terrain

The robot walked over gravles of calibrated size bought in a nearby home center. We tested several diameters with the **CDPG** Kajita et al. (2003a). The robot was able to walk on gravles of size up to $8\ mm$. Beyond this size, the robot was falling. Note that in Fig.13 the cost of transport is slightly more expensive that classical straight walking in nominal temperature, but not much that walking at $10°C$. It is far less expensive that climbing a slope or to counteract pushes. As expected it has no impact on the frequency of the footstep as can be see in the Froude Number.

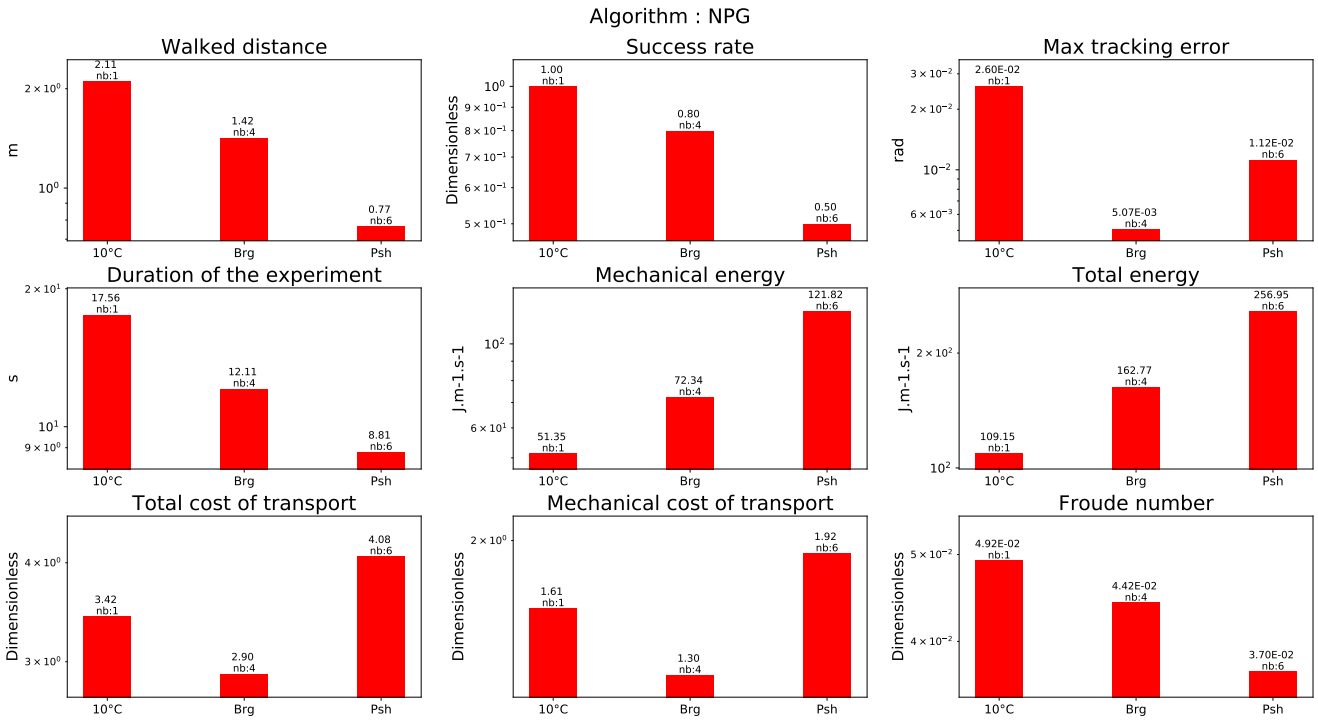

Figure 13. Straight walk with the walking pattern generator described in Naveau et al. (2017)

5.3.7 Walking over an obstacle

We have computed the same performance indicators for the behavior described in Koch et al. (2014) in the frame of the Koroibot project. This work is quite different from the others as it implements a **MPWBC** under the formulation of an Optimal Control Problem given by Eq.1. The solution of this problem was computed by the Muscod-II Diehl et al. (2001) solver. As the solver is trying to maximize a solution which is not on a reduced space (the centroidal dynamics for the previous algorithms) but on the whole robot, the solution find is near real constraints of the robot in terms of joint position, velocity, acceleration and torques. This is reflected in the cost of transport which is very high, 10.15, almost as high as the climbing stair of $15cm$ (see Fig.11-(muscode)).

5.4 Stabilizer

The stabilizer described in Kajita et al. (2007) and Kajita et al. (2001) was extremely resilient during all the tests. An horizontal plane generated oscillations along the sagittal plane and the perpendincular plane at $1\ Hz$ and $2\ Hz$ at various amplitude $[10, 20, 30, 40, 48]$ in mm. Along the sagittal plane at $40\ mm$ and $48\ mm$ for both frequencies the feet of the robot were raising. In the perpendicular plane at $40\ mm$ and $48\ mm$ for both frequencies the overall robot rotated of about $15°$ and $20°$. It was also tried to increase the frequency for a given amplitude of $10\ mm$. In the sagittal plane, the robot was able to reach $7\ Hz$ without falling. In the perpendicular plane at $7\ Hz$ the robot was making violent oscillations (without falling) reaching mechanical resonance. The trial was subsequently stopped. The results are depicted in Fig.14. We can clearly see that for the oscillation in the perpendicular plane the increase of total energy is following an exponential curve, compare to the same experience in the sagital plane. This clearly shows

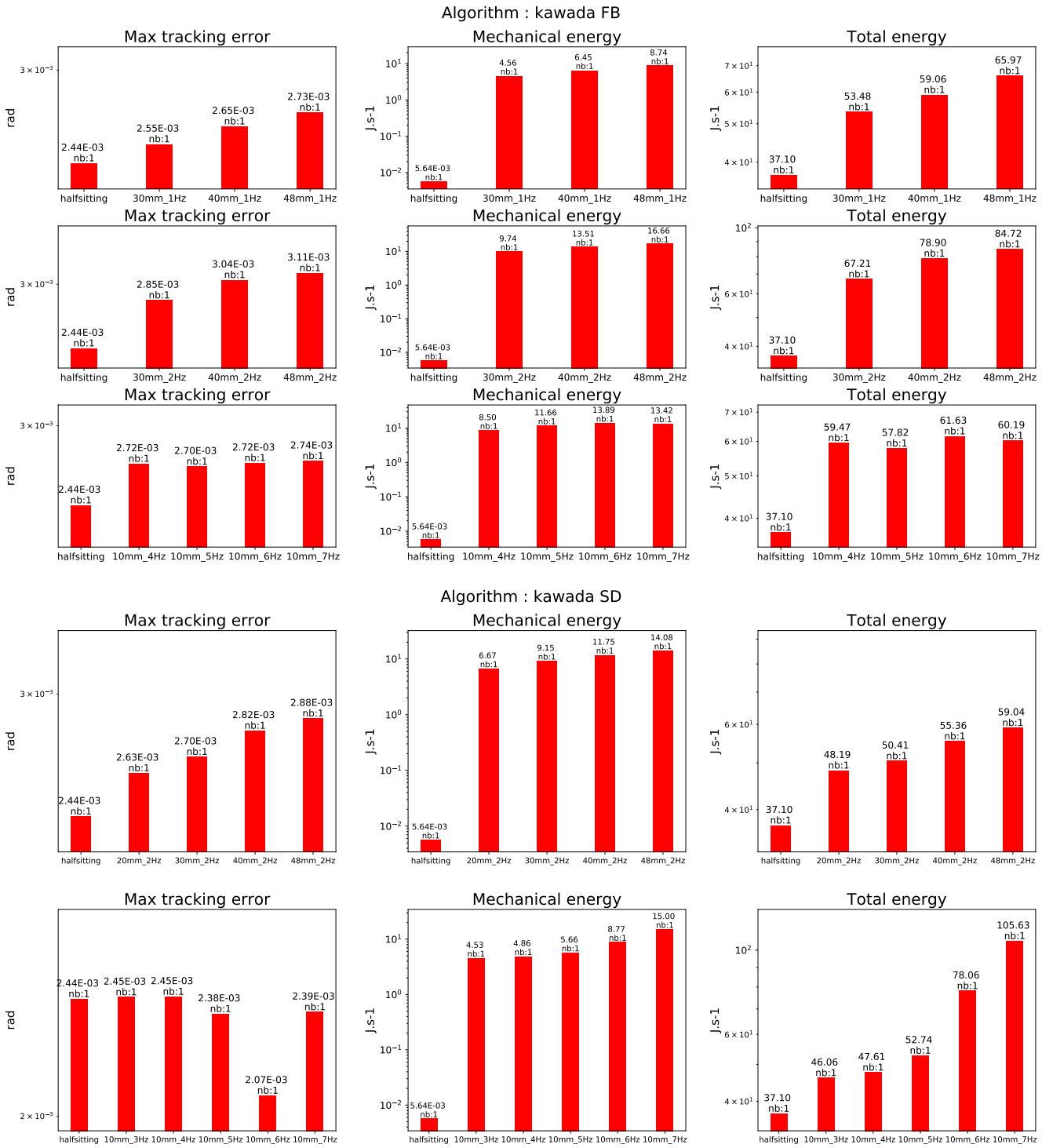

Figure 14. Stabilization evaluation of the algorithm described in Kajita et al. (2007) and Kajita et al. (2001). The upper figure show the results along the sagittal plane, whereas the lower figure depicts the results along the perpendicular plane.

that we reach the resonance frequence of the system as it can be seen in the video available at the following location https://www.youtube.com/watch?v=djWGsb44JmY&feature=youtu.be.

6 CONCLUSION

6.1 Summary and major outcomes

In this paper we presented a benchmarking for the control architecture such as the one in Fig.1 implemented on the HRP-2 robot owned by LAAS-CNRS. The performance indicator used in this paper are mostly based on Torricelli et al. (2015). Based on this work we computed the following set of KPI:

- walked distance,
- success rate,
- max tracking error,
- duration of the experiment,
- mechanical joint energy,
- actuators energy,
- cost of transport,
- mechanical cost of transport,
- Froude number.

They all represent either the particular characteristics of the experiments or the performance of the control architecture used.

The list of algorithms executed on the HRP-2 robot were:

- a flat ground capable **CDPG** from Kajita et al. (2003a),
- an analytical flat ground capable **CDPG** from Morisawa et al. (2007),
- a non linear flat ground capable **CDPG** from Naveau et al. (2017),
- a multi-contact **CDPG** from Carpentier et al. (2016),
- a **MPWBC** from Koch et al. (2014),
- a **WBC** which is the stabilizer from Kajita et al. (2007) and Kajita et al. (2001)
- a **WBC** that computes the joint position from the end-effector plus center of mass trajectories from Mansard et al. (2009)
- a **WBC** that computes the joint acceleration from the end-effector plus center of mass trajectories used in Carpentier et al. (2016)

The list of environmental conditions where the tests could successfully occur are:

- a temperature controlled room which provided from $10°C$ to $35°C$,
- a slope of various angles ($[1° - 3.0°]$),
- a controlled mobile platform that simulates a translating ground,
- a set of calibrated weight from $5\ kgs$ to $15\ kgs$,
- a stick with a force sensor on it to apply measured perturbation on the robot,
- different floors with different friction.

The list of the motion performed in the environmental conditions where:

- climbing up $10\,cm$ high stairs without handrail,
- climbing up $15\,cm$ high stairs with handrail,
- walking over stepping stones,
- walking on a beam,

- walking on a flat ground,
- walking on a slope,
- walking over obstacles.

From all these results and experiments few major results come out. First the temperature plays a roll on the energy consumed during a motion. We observed that the colder the room is the more mechanical and electrical energy is consumed. We also noticed that the more the motion is at the limit of stability the more the stabilizer has to inject energy into the system to compensate for potential drift. This create a noticeable increase in energy consumption, e.g. when the robot walk on a beam, step over obstacle, walk on stepping stones. However the most expensive motion is climbing stairs which is clearly a challenge for future potential applications where stairs are involved.

Finally in terms of cost of transport, the algorithm proposed by Carpentier et al. (2016) seems to be the most efficient and the most versatile. Its main disadvantage during this campaign was the lack of on-line implementation compare to Morisawa et al. (2007) and Naveau et al. (2017).

6.2 Future work

We could not properly compute the KPI when we tried to vary the friction of the ground. A future work is then to implement a proper slip observer like the one in Kaneko et al. (2005). Build a stabilizer that could be used in multi-contact in order to compensate for the external perturbation and the modeling assumption.

Furthermore, the LAAS-CNRS acquired a new humanoid robot Talos Stasse et al. (2017). The future work consist in implementing all the algorithms presented in this paper and perform the benchmarking on this new robot.

AUTHOR CONTRIBUTIONS

OS, EB, KGE conducted the experiments on the temperature, climbing stairs, at the LNE. MN and OS conducted the experiments with Koroibot. OS, EB and PS conceived the research idea. PS obtained funding for the project. OS, KGE, MN, EB, RG, GA and PS participated in the preparation of the manuscript.

ACKNOWLEDGMENTS

The financial support provided by the European Commission within the H2020 project ROBOCOM++ (JTC2016-PILOTS, Projet-ANR-16-PILO-0001) is gratefully acknowledged.

SUPPLEMENTAL DATA

As a reminder, a CAD model of the staircase used is available on the github repository where all the log of the experiments are also present: https://github.com/laas/koroibot_KPI. All the computation performed on the logs and implementing the key performance indicators are available here: https://github.com/laas/EnergyComputation.

REFERENCES

Brandao, M., Hashimoto, K., and Takanishi, A. (2017). Sgd for robot motion? the effectiveness of stochastic optimization on a new benchmark for biped locomotion tasks. In *Int. Conf. on Humanoid Robotics*

Carpentier, J., Tonneau, S., Naveau, M., Stasse, O., and Mansard, N. (2016). A Versatile and Efficient Pattern Generator for Generalized Legged Locomotion. In *Int. Conf. on Robotics and Automation*

Chestnutt, J. (2010). *Navigation and Gait Planning* (Springer London). 1–28

Clever, D., Harant, M., Mombaur, K., Naveau, M., Stasse, O., and Endres, D. (2017). Cocomopl: A novel approach for humanoid walking generation combining optimal control, movement primitives and learning and its transfer to the real robot hrp-2. *IEEE Robotics and Automation Letters* 2, 977–984

DeDonato, M., Polido, F., Knoedler, K., Babu, B. P. W., Banerjee, N., Bove, C. P., et al. (2017). Team wpi-cmu: Achieving reliable humanoid behavior in the darpa robotics challenge. *Journal of Field Robotics* 34, 381–399

Deits, R. and Tedrake, R. (2014). Footstep planning on uneven terrain with mixed-integer convex optimization. In *Int. Conf. on Humanoid Robotics*

del Pobil, A. P., Madhavan, R., and Messina, E. (2006). Benchmarks in robotics research. In *Workshop IROS*

Diehl, M., Leineweber, D. B., and Schäfer, A. (2001). *MUSCOD-II Users' Manual*. Universität Heidelberg

Grizzle, J. W., Chevallereau, C., Ames, A. D., and Sinnet, R. W. (2010). 3d bipedal robotic walking: models, feedback control, and open problems. *IFAC Proceedings Volumes*

Herdt, A., Perrin, N., and Wieber, P.-B. (2010). Walking without thinking about it. In *Int. Conf. on Intelligent Robots and Systems*

Iagnemma, K. and Overholt, J. (2015). Introduction. *Journal of Field Robotics* 32, 313–314. doi:10.1002/rob.21600

Johnson, M., Shrewsbury, B., Bertrand, S., Calvert, D., Wu, T., Duran, D., et al. (2017). Team ihmc's lessons learned from the darpa robotics challenge: Finding data in the rubble. *Journal of Field Robotics* 34, 241–261

Kajita, S., Kanehiro, F., Kaneko, K., Fujiwara, K., Harada, K., Yokoi, K., et al. (2003a). Biped walking pattern generation by using preview control of zero-moment point. In *Int. Conf. on Robotics and Automation*

Kajita, S., Kanehiro, F., Kaneko, K., Fujiwara, K., Harada, K., Yokoi, K., et al. (2003b). Resolved momentum control: Humanoid motion planning based on the linear and angular momentum. In *Int. Conf. on Intelligent Robots and Systems*

Kajita, S., Nagasaki, T., Kaneko, K., and Hirukawa, H. (2007). Zmp-based biped running control. *IEEE Robotics Automation Magazine* 14, 63–72

Kajita, S., Yokoi, K., Saigo, M., and Tanie, K. (2001). Balancing a humanoid robot using backdrive concerned torque control and direct angular momentum feedback. In *Int. Conf. on Robotics and Automation*. 3376–3382

Kaneko, K., Kanehiro, F., Kajita, S., Morisawa, M., Fujiwara, K., Harada, K., et al. (2005). Slip observer for walking on a low friction floor. In *Int. Conf. on Intelligent Robots and Systems*. 634–640

Koch, K. H., Mombaur, K., Stasse, O., and Soueres, P. (2014). Optimization based exploitation of the ankle elasticity of hrp-2 for overstepping large obstacles. In *Int. Conf. on Humanoid Robotics*

Koenemann, J., Del Prete, A., Tassa, Y., Todorov, E., Stasse, O., Bennewitz, M., et al. (2015). Whole-body model-predictive control applied to the HRP-2 humanoid. In *Int. Conf. on Intelligent Robots and Systems*

Kuindersma, S., Permenter, F., and Tedrake, R. (2014). An efficiently solvable quadratic program for stabilizing dynamic locomotion. In *Int. Conf. on Robotics and Automation*

Lim, J., Lee, I., Shim, I., Jung, H., Joe, H. M., Bae, H., et al. (2017). Robot system of drc-hubo+ and control strategy of team kaist in darpa robotics challenge finals. *Journal of Field Robotics* 34, 802–829

Mandery, C., Terlemez, O., Do, M., Vahrenkamp, N., and Asfour, T. (2016). Unifying representations and large-scale whole-body motion databases for studying human motion. *Transactions on Robotics*

Mansard, N., Stasse, O., Evrard, P., and Kheddar, A. (2009). A versatile generalized inverted kinematics implementation for collaborative working humanoid robots: The stack of tasks. In *Int. Conf. on Autonomous Robots*

Marion, P., Fallon, M., Deits, R., Valenzuela, A., Pérez D'Arpino, C., Izatt, G., et al. (2017). Director: A user interface designed for robot operation with shared autonomy. *Journal of Field Robotics* 34, 262–280

Mordatch, I., Todorov, E., and Popović, Z. (2012). Discovery of complex behaviors through contact-invariant optimization. *ACM Transactions on Graphics (TOG)*

Morisawa, M., Harada, K., Kajita, S., Nakaoka, S., Fujiwara, K., Kanehiro, F., et al. (2007). Experimentation of humanoid walking allowing immediate modification of foot place based on analytical solution. In *Int. Conf. on Robotics and Automation*

Mukovskiy, A., Vassallo, C., Naveau, M., Stasse, O., Soueres, P., and Giese, M. A. (2017). Adaptive synthesis of dynamically feasible full-body movements for the humanoid robot hrp-2 by flexible combination of learned dynamic movement primitives. *Robotics and Autonomous Systems* 91, 270–283

Naveau, M. (2016). *Advanced human inspired walking strategies for humanoid robots*. Ph.D. thesis, Université de Toulouse 3 Paul Sabatier

Naveau, M., Kudruss, M., and Stasse, O. (2017). A reactive walking pattern generator based on nonlinear model predictive control. *Robotics and Automation Letters* 2

Orin, D. E., Goswami, A., and Lee, S.-H. (2013). Centroidal dynamics of a humanoid robot. *Autonomous Robots* 35, 161–176

Perrin, N., Lau, D., and Padois, V. (2015). Effective generation of dynamically balanced locomotion with multiple non-coplanar contacts. In *the International Journal of Robotics Research*

Qiu, Z., Escande, A., Micaelli, A., and Robert, T. (2011). Human motions analysis and simulation based on a general criterion of stability. In *International Symposium on Digital Human Modeling*

Radford, N. A., Strawser, P., Hambuchen, K., Mehling, J. S., Verdeyen, W. K., Donnan, A. S., et al. (2015). Valkyrie: Nasa's first bipedal humanoid robot. *Journal of Field Robotics* 32, 397–419

Rotella, N., Herzog, A., Schaal, S., and Righetti, L. (2015). Humanoid momentum estimation using sensed contact wrenches. In *Int. Conf. on Humanoid Robotics*

Sherikov, A. (2016). *Balance preservation and task prioritization in whole body motion control of humanoid robots*. Ph.D. thesis, INRIA

Sherikov, A., Dimitrov, D., and Wieber, P.-B. (2014). Whole body motion controller with long-term balance constraints. In *Int. Conf. on Humanoid Robotics*

Spenko, M., Buerger, S., and Iagnemma, K. (2017). Editorial. *Journal of Field Robotics* 34, 227–228. doi:10.1002/rob.21711

Stasse, O., Flayols, T., Budhiraja, R., Giraud-Esclasse, K., Carpentier, J., Prete, A. D., et al. (2017). Talos: A new humanoid research platform targeted for industrial applications. In *IEEE/RAS Int. Conf. on Humanoid Robotics (ICHR)*

Takumi, K., Hiroyuki, K., Mitsuhide, K., Chiaki, T., Shinya, S., Masanori, T., et al. (2017). Dynamic gait transition between walking, running and hopping for push recovery. In *Int. Conf. on Humanoid Robotics*

Tassa, Y., Mansard, N., and Todorov, E. (2014). Control-limited differential dynamic programming. In *Int. Conf. on Robotics and Automation*

Torricelli, D., González-Vargas, J., Veneman, J.-F., Mombaur, K., Tsagarakis, N., del Ama, A. J., et al. (2015). Benchmarking bipedal locomotion: A unified scheme for humanoids, wearable robots, and humans. *IEEE Robotics Automation Magazine*

Tsagarakis, N. G., Caldwell, D. G., Negrello, F., Choi, W., Baccelliere, L., Loc, V., et al. (2017). Walkman: A high-performance humanoid platform for realistic environments. *Journal of Field Robotics* 34, 1225–1259

Westervelt, E. R., Grizzle, J. W., Chevallereau, C., Choi, J. H., and Morris, B. (2007). *Feedback control of dynamic bipedal robot locomotion* (CRC Press)

Wieber, P.-B. (2008). Viability and predictive control for safe locomotion. In *Int. Conf. on Humanoid Robotics*

Wieber, P.-B., Tedrake, R., and Kuindersma, S. (2015). *Handbook of Robotics* (Cham: Springer), chap. Modeling and Control of Legged Robots